ELSEVIER

Journal of Crystal Growth 169 (1996) 649–659

JOURNAL OF CRYSTAL GROWTH

# Comparison of the crystalline quality of step-graded and continuously graded InGaAs buffer layers

P. Kidd [a,*], D.J. Dunstan [b], H.G. Colson [b], M.A. Lourenço [c], A. Sacedón [d], F. González-Sanz [d], L. González [e], Y. González [e], R. García [e], D. González [f], F.J. Pacheco [f], P.J. Goodhew [g]

[a] Department of Materials Science and Engineering, University of Surrey, Guildford, GU2 5XH, UK
[b] Department of Physics, University of Surrey, Guildford, GU2 5XH, UK
[c] Department of Electronic and Electrical Engineering, University of Surrey, Guildford, GU2 5XH, UK
[d] Departamento Ingeniería Electrónica, E.T.S.I. de Telecomunicación, Cuidad Universitairia, 28040 Madrid, Spain
[e] Centro Nacional de Microelectrónica (CSIC), Serrano 144, 28006 Madrid, Spain
[f] Departamento de Ciencia de los Materiales e IM y QI, Universidad de Cádiz, Apartado 40, 11510 Puerto Real (Cádiz), Spain
[g] Department of Materials Science and Engineering, University of Liverpool, Liverpool, L69 3BX, UK

Received 22 January 1996; accepted 14 June 1996

**Abstract**

In this paper we summarize work carried out to investigate the relaxation of epitaxial strained layers of InGaAs on GaAs, where the InGaAs composition has been increased throughout the layer in either a stepwise or linearly graded form. The results are presented from the viewpoint of exploiting the relaxed layers to provide prescribed in-plane surface lattice parameters for subsequent use as "virtual" substrates for novel devices. We compare the behaviour of step-graded and linearly graded InGaAs layers. We consider the crystalline quality of different structures and discuss the design requirements for subsequent device quality growth.

## 1. Introduction

Relaxed buffer layers are required in semiconductor epitaxy to achieve an in-plane lattice constant different from those available on high-quality large-area commercial substrates such as Si, GaAs and InP. An enormous effort has been put into developing such layers over the years, and relaxed GaAs grown on silicon is now commercially available. Several strategies may be identified in the literature including simple constant composition layers, linearly graded layers, step-graded layers, and more complicated structures including, for example, superlattices (for a review see Ref. [1]). No systematic study has been reported in which these different strategies are properly compared, and from the theoretical point of view it is unclear how the different strategies should perform. Linear grades and step grades are the two simplest ways of controlling the misfit at the growth surface. Both reduce the threading dislocation density compared with structures such as single high mismatch composition layers.

We present results from a systematic study of

* Corresponding author.

0022-0248/96/$15.00 Copyright © 1996 Elsevier Science B.V. All rights reserved
PII S0022-0248(96)00665-3

simple graded structures, using two growth techniques, molecular beam epitaxy (MBE) and atomic layer molecular beam epitaxy (ALMBE), for comparison. We report analysis of the plastic relaxation behaviour and crystal quality of stepped and linear graded buffer layers. We investigate the following phenomena which are associated with the process of strain relaxation in epitaxial layers; predictability of relaxation and control of surface lattice parameter, depth of dislocation-free material below the top surface, number of threading dislocations, height of surface striations and layer tilt. We discuss the effects of different buffer layer structures on these parameters.

## 2. Theory

We have developed a method for measuring and predicting the macroscopic strain in relaxed buffer layers. It is based on the empirical observation that relaxing layers will tend to relax to a residual strain-thickness product given by

$$\epsilon h = k. \quad (1)$$

Here $\epsilon$ is the average layer strain, which we define as

$$\epsilon = (a_{\parallel} - a_x)/a_x,$$

where $a_{\parallel}$ is the measured in-plane lattice parameter of the alloy layer, and $a_x$ is the bulk lattice parameter of the same alloy in its fully relaxed state. $h$ is the layer thickness and $k$ is an empirical constant [2]. In our work on InGaAs layers on (001) oriented GaAs substrates, we have found that the constant $k$ takes the value $0.8 \pm 0.1$ nm. Whilst the exact physical significance of this law has not been wholly proven, the law nonetheless holds true for $In_xGa_{(1-x)}As$ layers grown on GaAs, providing the growth is well controlled 2D layer-by-layer growth [2–5]. In practice we have found that this means that the "growth strain" must not exceed 0.018 for MBE growth, or 0.035 for ALMBE growth. We define the "growth strain" as the misfit of newly deposited material with respect to the surface on which it is being deposited, and is not to be confused with the more general term "misfit", which often alludes to the difference between the in-plane lattice parameter of the layer at thickness $h$ and the substrate.

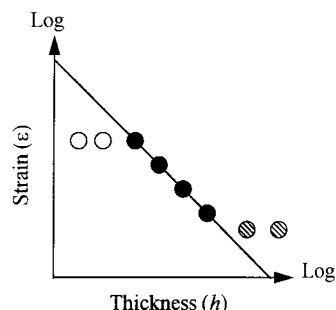


Fig. 1. Schematic diagram illustrating the law: $\epsilon = k/h$ (line) with reference to samples: (open circles) below relaxation critical thickness, (closed circles) relaxing according to the law and (shaded circles) exhibiting small residual strain.

The observation that this law applies only to samples which have satisfied stringent growth requirements implies that we are confining the law to samples which relax according to the same strain-relief mechanisms. That is, the "good growth" condition, which is an empirical result, is effectively limiting the available strain relief mechanisms to one or a small number of reproducible types (including, for example nucleation and glide of 60° dislocations) and any other growth conditions, e.g. 3D growth, could include the nucleation of other strain relief mechanisms which would compromise this predictability [5,6]. For example, Drigo et al. have presented an empirical relation based on an apparent $h^{1/2}$ dependence of strain [7], this does not disprove our law since we would argue that this dependence, which does not discriminate for layer growth quality, possibly includes layers where a greater variety of strain relief mechanisms are operational.

Fig. 1 illustrates the law for a general graded structure, and summarizes the behaviour observed for over 50 samples, both single composition layers and stepped and linear grades, the data for which have been published elsewhere [2–5]. The empirical law is true in principle for compositions of $In_xGa_{(1-x)}As$ with $x$ up to 1, although we have only proven it to be true for grades with $x$ up to 0.6. For structures other than single layers, consisting of $n$ layers, the strain corresponds to the average strain for the structure and the thickness to the total thickness

$$\epsilon = \Sigma^n h_i \epsilon_i / \Sigma^n h_i, \quad (2)$$

$$h = \Sigma^n h_i. \quad (3)$$

Several useful predictions arise from the empirical law. Relaxation occurs only for layers with strain thickness products exceeding $k$. The open circles in Fig. 1 illustrate the strain values for layers whose strain-thickness products are below $k$. On exceeding the critical strain-thickness product any layer structure will then relax until its strain thickness product is reduced to the value $k$. Such relaxed layers are represented by the filled circles in the figure. The only significant deviation measured experimentally is illustrated in Fig. 1 by the shaded circles. It has been found that, where near-zero residual strain is predicted, for thick layers, small residual strains, $\epsilon < 0.0001$, are often observed. This provides us with a lower limit estimate of the residual strain that might remain in the relaxed region of a buffer layer structure.

This empirical law therefore allows us to predict the final average strain integrated over the whole of the epitaxial layer structure. Fig. 2a–2c show schematic representations of unrelaxed structures defined by their composition and thickness (single lines referred to composition scale) which have been "relaxed" (bold lines referred to strain scale) such as to give an integrated strain-thickness product where $\epsilon h = k$. We predict that misfit dislocations will be present at the lowest possible position in the structure, so that any remaining strain is therefore in the top dislocation-free layers with thickness $Z$. This is illustrated by the shaded area under the bold lines, which exists at the top of the structure and has the value $k$. Any structure can thus be "relaxed" theoretically so that its final strain-thickness product $= k$. From this the in-plane lattice parameter at the top surface can be calculated. Details of this theoretical process have been presented elsewhere [8,9].

At a distance below the surface greater than $Z$, it is assumed that the net residual strain is zero. This is almost upheld in practice, and measurements of $Z$ in our structures are always close to that predicted by the model. Occasionally the measurement of $Z$ is less than predicted [10,11] but this is accompanied by a small measurable residual strain in the layers at depths greater than $Z$, rendering the final average strain-thickness product equal to $k$.

In Section 4 we present results which illustrate this law for three structures. Then, within the regime of this law, we present results of investigations into the crystal quality of different buffer layer structures to find out which, if any, of the details of the buffer layer design are significant for overall crystal quality.

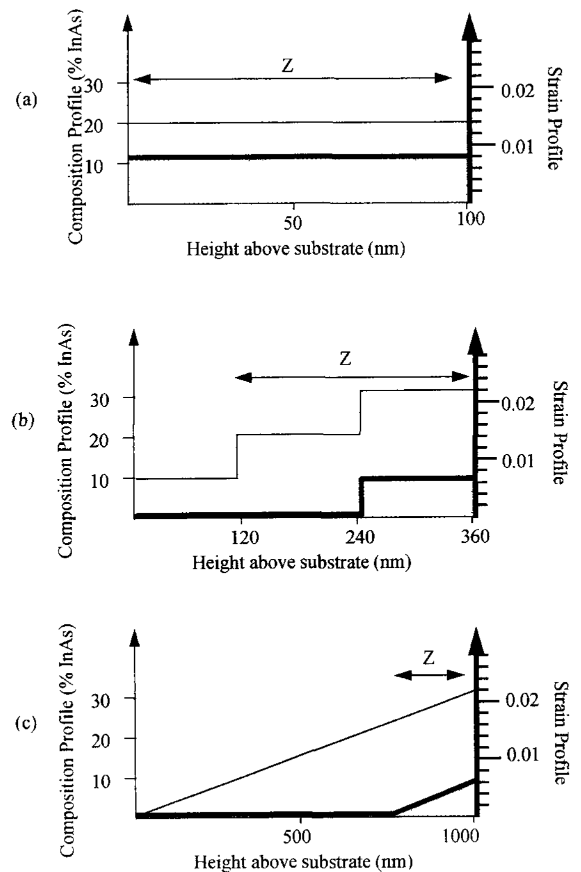


Fig. 2. Schematic representations of (a) single, (b) step-graded, and (c) linearly graded, buffer layer structures showing composition profile (single line and scale) and predicted strain after relaxation (bold line and scale). The structures are predicted to relax to give a strain thickness product $\epsilon h = k$, where $k$ is illustrated by the shaded region. It is predicted that there will be a dislocation-free region above a depth $Z$ below the surface.

## 3. Experimental procedure

### 3.1. Growth

Samples were all $In_xGa_{(1-x)}As$ alloys grown by MBE and ALMBE on nominally exact (001) semi-

insulating GaAs wafers. For molecular beam epitaxy (MBE), the GaAs growth conditions were growth at 500°C, at a rate of 0.7 $\mu$m/h with a V/III beam flux ratio of 3 using $As^4$. For the linear grades the GaAs growth rate was kept constant and the InAs growth rate was changed, giving a total growth rate changing from 0.7 to approximately 1.5 $\mu$m/h for a grade up to 50% InAs. For atomic layer molecular beam epitaxy (ALMBE) [12] the layers were grown at 400°C with a growth rate of 1 monolayer per second.

Table 1
Estimate of variation in measurements for relaxed layers

| Technique | Measurement | Symbol ± variation |
|---|---|---|
| Plan-view TEM | Misfit dislocation density | md $\pm 10^4$ $cm^{-1}$ |
| Cross-section TEM | Layer thickness | $h \pm 5$ nm |
| Cross-section TEM | Threading dislocation density | td $\pm 10^5$ $cm^{-2}$ |
| X-ray diffraction | Composition | $x \pm 0.01$ |
| X-ray diffraction | Strain | $\epsilon \pm 0.001$ |
| Talistep | Mean striation height | $s \pm 4$ nm |
| AFM | Mean striation height | $s \pm 2$ nm |

### 3.2. Analysis

Mean composition and residual strain were measured from the layer-peak to substrate-peak splitting, for the symmetric 004 and asymmetric 115 reflections, using double crystal X-ray diffraction (DCXD) as described previously [4]. In the case of step-graded layers, strains could only be measured for layers where the layer peak position could be unequivocally identified for all Bragg reflections. The success of this measurement depended on the extent of peak broadening and overlap due to tilting in the layers as described later. For the graded layers it was possible to measure the residual strains in the constant composition caps on the top of some of the layers. Where TEM showed no dislocations at the grade/cap interface, the surface lattice parameter of the grade could then be inferred. For one of the graded layers, which was examined using triple axis diffractometry, an approximate measure of the strain in the top, undislocated, part of the grade was obtained by virtue of a small peak on the tail of the diffraction profile from the grade.

Assessment of microstructure, layer thickness and dislocation content was carried out using plan-view and cross-sectional transmission electron microscopy (PTEM and XTEM). High resolution X-ray reciprocal space mapping [13] was used to measure residual strain in the graded layers, and to study mosaic spread and microscopic tilting. Surface morphology was studied by Talysurf, AFM or Nomarski microscopy.

In all cases, for our measurements, the precision of the experimental techniques was far greater than the spread in values arising from the inhomogeneous distribution of defects in the samples. Our approach was to build up a picture of the variation from the mean by taking all our measurements from many samples, rather than undertaking detailed statistical measurements from one or two samples. Table 1 gives an estimate of the precision of the measurements from each technique. This value arises, not from the instrument function for each method, but as a result of the spread in measurements resulting from the relaxation process itself.

### 3.3. Samples

We have grown and investigated more than 20 step-graded and linearly graded samples. Those presented here typify the trends observed overall. Our previous studies were performed on single constant composition, "flat" layers with compositions $In_xGa_{(1-x)}As$ such that $x < 0.3$ [2]. Here we have investigated samples with multiple flat layers, usually with increasing composition, typically in steps of $x = 0.1$. We have also examined linearly graded layers with grade rates $x/h$ (%InAs/nm) in the range 0.03%/nm to 0.13%/nm.

## 4. Results

### 4.1. Strain measurements

Step- and linearly graded layers both relax according to our empirical law [2]. Table 2 gives the measurements obtained for a typical flat layer, a step

Table 2
Comparison of measured and predicted strain in typical single layer, step-graded and linearly graded epitaxial layers

| Structure | $x$% InAs | $h$ (nm) | $\epsilon$ measured | $\epsilon$ predicted |
|---|---|---|---|---|
| Single layer | 20 | 100 | 0.008 | 0.008 |
| Step-graded | | | | |
| Layer 1 | 10 | 120 | 0.000 | 0.000 |
| Layer 2 | 20 | 120 | 0.001 | 0.000 |
| Layer 3 | 30 | 120 | 0.005 | 0.006 |
| Linear grade | | | | |
| Start | 0 | | | |
| Finish | 30 | 1000 | 0.003 | 0.003 |

grade and a linear grade. These structures are depicted schematically in Figs. 2a–2c. Fig. 3 and Fig. 4 show typical cross-section TEM images for the step grade and the linear grade, respectively.

For the flat layer the misfit dislocations are confined to the interface region [4]. The predicted and measured residual strains agree.

For the 3-step grade in Fig. 3, the majority of the misfit dislocations are confined to the step interfaces with some dislocation segments passing between the interfaces. The residual strain averaged over the whole structure is in agreement with the model. However, regarding the individual layers, there is some small residual strain in the middle layer. We would expect that dislocations would not be positioned above regions of strain, i.e. the third interface should only contain dislocations when the second layer is at zero strain. However, for our sample it appears that there are not enough dislocations present at the lower interfaces to achieve full relaxation of the lower layers, but for the overall structure this is compensated by the presence of a few dislocations in higher layers. This behaviour is typical for step-graded layers and will be discussed further in the next section.

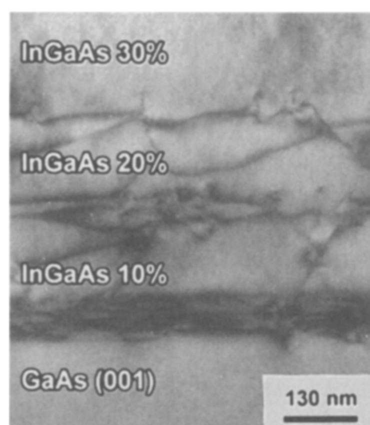


Fig. 3. TEM cross-section image showing the step-graded structure depicted in Fig. 2b.

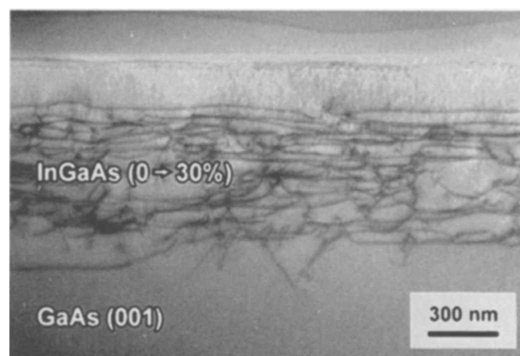


Fig. 4. TEM cross-section image showing the linearly graded structure depicted in Fig. 2c.

For the linear grade in Fig. 4, the dislocations are spread throughout the grade with a dislocation-free region, with thickness 200–250 nm, at the top of the grade. Although we cannot measure the strain in the lower parts of the structure, our model predicts that the top of the grade will have an average residual strain 0.003 distributed over a depth 270 nm. Measurement of the residual strain, using reciprocal space mapping, gives a value of $0.003 \pm 0.001$ in remarkably good agreement with the model.

Whilst the top layer in the structure will be grown with composition $x$, the effect of the compressive strain is such that there will be an in-plane lattice parameter equivalent to a composition $x'$ where $x' < x$. Matching an unstrained capping layer to the in-plane lattice parameter of a graded buffer has been illustrated using a series of samples with varying cap composition. This has been reported elsewhere [8,10].

In summary, on relaxing a step- or linearly graded layer there is always a dislocation-free region in the top of the buffer layer. This region contains most of the strain in the structure, and the strain-thickness product for this region is approximately $0.8 \pm 0.1$

nm. In some cases small residual strain is present in the lower regions of the layers. Regarding in-plane lattice constant, we are thus confident that for our structures the final in-plane lattice constant is predictable to within 0.1% (1000 ppm).

### *4.2. Misfit dislocation distribution and the depth, z, of dislocation-free material below the top surface*

Using cross-section TEM the distribution of misfit dislocations with depth can be easily observed. The main differences between linearly graded and step-graded layers, from this viewpoint, are typified by the two micrographs shown in Figs. 3 and 4. The effect of having composition steps and constant composition layers in the structure is to confine the misfit dislocations to the interfacial regions between the layers. It has been suggested previously, [16], that the residual strain in the lower layers was due to dislocation pinning by the compositionally abrupt interface. We tested this hypothesis by growing a two-step grade consisting of two 120 nm thick layers of InGaAs with compositions $x = 0.1$ and 0.2, in one case with an abrupt interface, and in a second case with the interface graded over a region with thickness 66 nm. Despite having a graded interface, the second sample still had dislocations lying in the interfaces and still exhibited a small, but measurable residual strain in the lower layer. We conclude that, rather than a mechanism of pinning at the interface, it is the presence of a constant composition (thus constant strain), thick layer which, at low stresses, is unable to provide sufficient driving force to send the last misfit dislocations to the interface in order to achieve complete relaxation. This effect was observed in both MBE and ALMBE layers.

Linear grades appear to have the advantage of spreading the misfit dislocations with depth throughout the layer. It has often been assumed, that because of this the graded layers must achieve full relaxation [17], but the evidence for lattice composition and relaxation at all depths in a grade is not easily obtainable. Grading from $x = 0$ at the GaAs substrate surface appears to allow dislocations to penetrate into the substrate, an effect which is evident in Fig. 4 and which has been reported elsewhere [18].

Near to the top of linear grades, where the residual strain is small, (i.e. $\sum \epsilon h = 0.8$ nm), no further relaxation will take place, leaving a strained and dislocation-free region at the top of the grade. Step grades made of constant composition layers necessarily have a dislocation-free region near to the top, which is the thickness of the top layer. In this sense the depth below the surface of the nearest misfit dislocation is readily controllable.

In summary, in terms of the misfit dislocation distribution, constant composition layers can be used to locate dislocations into well-defined regions. Linear grades can be used to spread them out. Abrupt composition steps can be useful to prevent dislocations from penetrating too deeply into a structure, and would be particularly useful at the beginning of a linear grade.

### *4.3. Threading dislocations*

If threading dislocations can be easily observed in a cross-section TEM sample then, even though the sampling volume is very small, this gives a lower limit to their density (approximately $10^5$ cm$^{-2}$). Conversely, the absence of threading dislocations gives the same value as an upper limit on the threading dislocation density. When threading dislocations are observed, the sampling volume in cross section is prohibitively small for good statistics to be applied in the analysis, but estimates to within an order of magnitude are useful. Measurement of threading dislocation density by plan-view TEM is often difficult because the density of dislocations lines in misfit dislocation arrays often makes it difficult to identify threading "ends" over a large enough area. Whether this measure of threading dislocation density is a significant indication of whether the buffer layer is suitable for subsequent device fabrication remains to be proven. For all the structures that we have studied, where the behaviour is according to the empirical relaxation curve, provided the growth strain does not exceed 1.8%, and that growth is well controlled, there is no other significant design factor which can be identified as causing a noticeably high density of threading dislocations, i.e. the threading dislocation densities have always remained less than $10^5$ cm$^{-2}$ [11,14]. When growth strains exceed 1.8% a high density of threading dislocations ($> 10^8$ cm$^{-2}$) is invariably observed [14,15].

### 4.4. Surface striations

There are many studies of surface structure in relaxing layers (for a review see Ref. [19]). The surface features are treated as a phenomenon resulting from varied growth rates on surfaces experiencing plastic relaxation. In our previous work, for constant composition single layers, we identified that for MBE growth, the presence of clear cross-hatch is indicative of good 2D growth and predictable relaxation and that any other surface feature is indicative of growth problems and results in unpredictable relaxation [5]. Beanland et al. [20] have characterized the shape of the striations and compared their positions with those of dislocation groups in the underlying array. We showed previously that the amplitude of growth striations appears to be reduced by growth at lower temperatures [4].

Table 3 summarizes the results of some surface studies of step-graded and linearly graded layers grown by MBE and ALMBE, and measured by Talisurf (T) and AFM single scans (S) and AFM line-scan averaging (A). It is not possible to simply compare measurements from the two techniques, but each are useful to identify general trends.

For the linear grades grown by MBE, the mean striation height, as measured by Talisurf, increases with thickness and relaxed strain. Samples G3280-2 (ALMBE) and G3281-2 (MBE) show that for similar sample structures the striation height is generally lower for ALMBE growth than MBE growth. However, care has to be taken in gathering the measurements as shown. The single scan AFM measurements for G3280-1 and G3281-2, along the $[\bar{1}10]$ azimuth, reveal that striation heights from both growth techniques appear similar. However, along the [110] direction, the striations on the MBE grown sample are much greater. This strong asymmetry in striation height is commonly observed on MBE samples and has been attributed to the often observed asymmetry in the densities of dislocations running along the two orthogonal interfacial ⟨110⟩ type directions [20,21]. The results for the ALMBE step-graded layers show that generally we should expect the striation height to increase with thickness and relaxation, but we have not identified a simple relationship between striation height and strain or thickness. Preliminary work has shown that extreme care has to be taken to interpret roughness measurements. Often the striations show an asymmetric nature. Also, by averaging several line scans over an area of surface quite a different apparent height can be measured as illustrated for samples G3175-2, G3176-2 and G3232-1 in Table 3, we are therefore reluctant to draw comparisons between surfaces measured by different techniques without further analysis.

Striations are a necessary consequence of controlled relaxation. We observed that, within a given growth regime, whether a structure is step-graded or linearly graded, provides no distinct advantages with regard to reducing the height of striations. However, the overall layer thickness should be minimized. By continuing to grow lattice-matched InGaAs on a striated InGaAs by MBE we have observed that the height of the striations increases further. Generally, reduced striation heights can be achieved by a differ-

Table 3
Measurement of surface striation height

| Sample | Description | Total thickness $h$ (nm) | Relaxed strain $\Delta\epsilon$ | Striation height talisurf (nm) [0°]/[90°] | Striation height AFM(S) (nm) [110]/$[\bar{1}10]$ | Striation height AFM(A) (nm) [110]/$[\bar{1}10]$ |
|---|---|---|---|---|---|---|
| #321 (MBE) | Linear grade $x$ from 0% to 30% | 185 | 0.007 | 2/1 | | |
| #324 (MBE) | Linear grade $x$ from 0% to 30% | 339 | 0.009 | 2/1 | | |
| #237 (MBE) | Linear grade $x$ from 0% to 30% | 1000 | 0.018 | 9/3 | | |
| G3280-2 (ALMBE) | Single layer $x = 20\%$ | 400 | 0.010 | | 5.8/3.3 | 4.8/1.8 |
| G3281-2 (MBE) | Single layer $x = 20\%$ | 400 | 0.010 | | 21.5/4.9 | 17.2/2.3 |
| G3175-2 (ALMBE) | Two-step grade $x = 10\%, 20\%$ | 240 | 0.007 | | 3 (Ave) | 1.8 (Ave) |
| G3176-2 (ALMBE) | Three-step grade $x = 10\%, 20\%, 30\%$ | 360 | 0.015 | | 3 (Ave) | 1.5 (Ave) |
| G3232-1 (ALMBE) | Five-step grade $x = 10\%, 20\%, 30\%, 40\%, 50\%$ | 600 | 0.038 | | 10 (Ave) | 4.6 (Ave) |

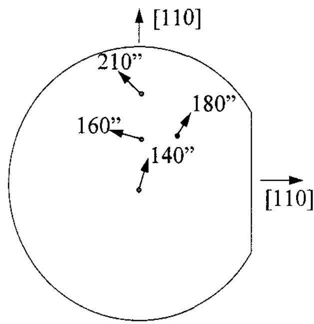


Fig. 5. Schematic plot of tilt (arcsec) and direction of maximum tilt (arrow) for a relaxed layer measured by DCXD at different positions on a wafer substrate.

ent growth mode, for example with a technique such as ALMBE.

### 4.5. Layer tilt

Relaxation of strained layers is almost always accompanied by macroscopic tilting of the layers. It is generally assumed that the magnitude and direction of the tilt is a function of the statistics of the underlying dislocation array. We have found for MBE layers that the major tilt axis for a sample is not predictable, neither is the magnitude of tilt. Both magnitude and direction may vary from region to region on a wafer. Fig. 5 shows a position plot of tilt direction and magnitude for a single relaxed 200 nm thick layer of $In_{0.2}Ga_{0.8}As$ on a GaAs wafer.

Fig. 6a shows a series of 004 (symmetric reflection) rocking curves taken at four orthogonal azimuths along the wafer for a step-graded sample with five layers. As shown schematically in Fig. 6b, each layer is tilted in the same sense with respect to the previous. The tilt with respect to the substrate is thus increasing as the layer is grown thicker. This has been observed to be the general behaviour of both step- and linearly graded layers. For the 270° azimuth the tilt is in the same sense as the change in Bragg angle and thus increases the peak splitting. For the 90° azimuth the tilt is opposite to the shift in Bragg angle bringing all the layer peaks to a point of coincidence with the substrate peak. Along the 0° and 180° azimuths, which happen, in this case to be normal to the major tilt axis, there is no measured layer tilt. As it happens, each of the layer peaks overlaps, making measurement of strain in this azimuth difficult.

For ALMBE layers the tilt axis is predominantly along the [110] azimuth, although the reason for this is not yet clear.

Tilt can be more readily measured using reciprocal space mapping. Fig. 7a–7c and Fig. 8 show reciprocal space maps (RSMs) about the 004 Bragg peaks for four samples. Fig. 7a corresponds to a

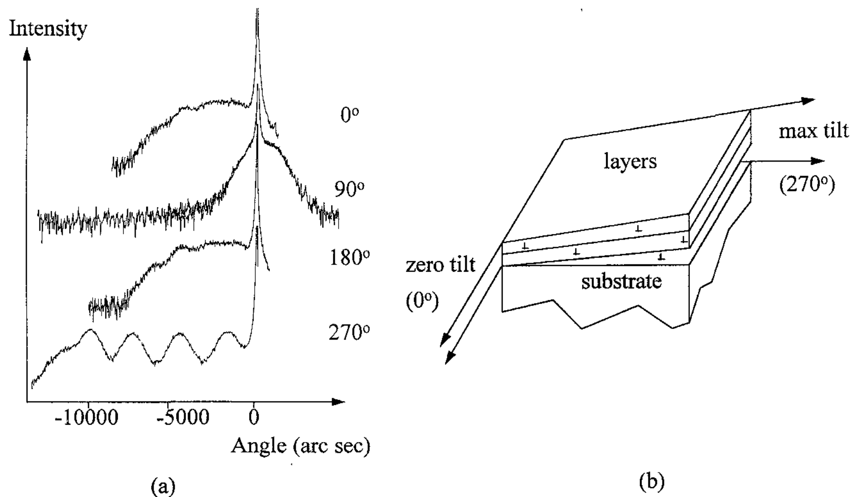


Fig. 6. (a) DCXD rocking curves about the 004 Bragg peak for a 5-step grade, taken at 4 orthogonal azimuths. (b) Schematic diagram of the buffer layer tilt referred to the measured azimuths in (a).

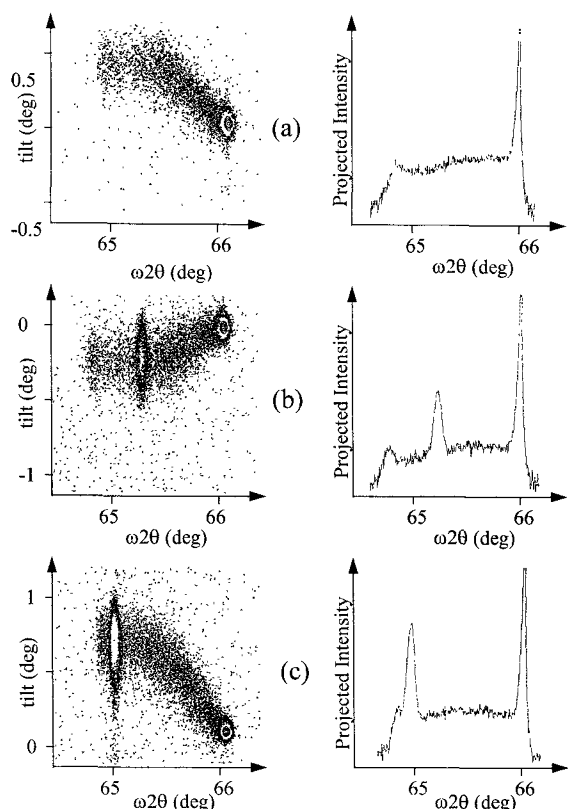


Fig. 7. Reciprocal space maps and associated projected intensity profiles for three graded layer structures: (a) linear grade from $x = 0$ to $x = 0.3$ over 1000 nm. (b) As (a) with a 300 nm cap with $x = 0.0.22$. (c) As (a) with a 500 nm cap with $x = 0.27$.

linearly graded layer grown by MBE with composition grade from $x = 0$ to $x = 0.3$ over 1000 nm. Fig. 7b corresponds to a sample with the same grade and a 300 nm constant composition ($x = 0.22$) cap. Fig. 7c again corresponds to the same grade with a 500 nm constant composition ($x = 0.27$) cap. Fig. 8 corresponds to a step-graded structure, with 6 layers each 120 nm thick and with compositions increasing from $x = 0.1$ to $x = 0.6$, followed by a 1000 nm thick InP capping layer. The RSM can be used to investigate lattice parameter ($\omega 2\theta$ axis) and tilt ($\omega$ axis). The accompanying graphs show the total intensity in the maps projected onto the $\omega 2\theta$ axis. The largest peaks correspond to the substrates and the next highest are from the capping layers. There is a broad peak from the grade and a small peak at the end of each grade. We interpret this to correspond to diffraction from the dislocation-free region at the top of the grade. Macroscopic tilting is measured directly on the reciprocal space map as a shift of the Bragg peak along the tilt axis. This corresponds to the mean tilt of the layer volume being sampled (a few $mm^2 \times$ layer thickness). As can be seen from the reciprocal space maps, all the samples under study are tilted. For the graded layers and the step-graded layers the tilt is increasing cumulatively as the layer thickness increases. We have never observed a change of tilt direction with depth. Tilts can range from a few hundred arcsec to values of 1 or 2 degrees in the thicker grades. The tilt is greatest at the beginning of the grade and stops increasing towards the top of the grade, presumably as the dislocation density reduces.

Whilst macroscopic tilting gives rise to a shift of the Bragg peak along the tilt axis, microscopic variations in tilt give rise to spreading of the peak along the tilt axis [22,23]. Thus a narrower peak along the tilt axis corresponds to a more uniform layer. It is interesting to note for the linearly graded layers in Fig. 7 and the step-graded layer in Fig. 8, that the top capping layer takes on the tilt of the macroscopic tilt of the structure, but that for the thicker caps, the

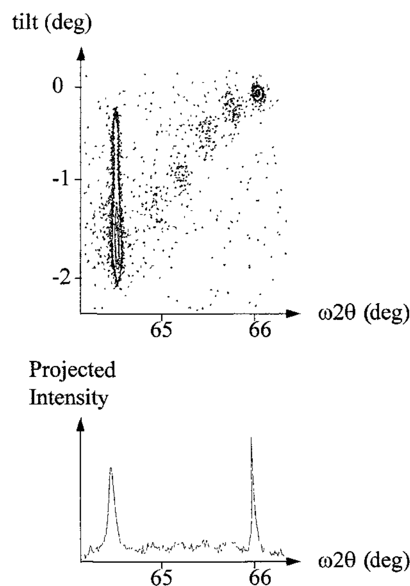


Fig. 8. Reciprocal space map and projected intensity profile for a 6-step grade with $x$ increasing from 0.1 to 0.6, and each layer thickness 120 nm and with a 1000 nm InP cap.

Bragg peak spreads out towards the zero tilt axis. One interpretation of this is that the capping layer is "recovering" the original lattice orientation, but a mechanism for how this might be achieved is not yet understood.

In summary, tilting is a consequence of the relaxation of the layers. The axis of tilt appears to be random for MBE layers, but consistently aligned along the [110] azimuth for ALMBE layers. The reasons for this are not understood. Tilt generally increases throughout a structure as more dislocations are introduced. Once established, the sense of tilt stays the same throughout the structure. There is no obvious distinction between step grades and linear grades with regard to the formation and magnitude of the layer tilt. We have not identified a method for predicting the direction and extent of the macroscopic tilting. Whilst tilt is readily measurable it has yet to be established whether layer tilting is of any consequence to subsequent device quality.

### 4.6. Critical grade rate

We observed with single layer samples that good growth was only possible when the growth strain (i.e. mismatch at the growth interface) is less than 0.018 and also that a layer will only relax when its strain-thickness product exceeds 0.8 nm, at which point it will relax so as to maintain this value. These facts together allow us to calculate a critical grade rate for stepped or linear grades. The calculation is not trivial since the state of strain at the growth interface has to be calculated in the light of change in relaxation as the total layer thickness increases. The design and calculation of strain relaxation of linear grades has been discussed elsewhere [8,10] and the design of more complicated structures has been presented by Dunstan [9].

Fig. 9 shows schematically the considerations that we apply in designing the best grade rate. We have found for linear grades that growth at the critical grade rate, which is the fastest rate in principle and is shown by the solid black line, is in practice too fast for good quality layers, since if for any reason relaxation is not immediate the 2D–3D growth threshold is rapidly reached. This is identified by a sudden increase in the number of threading dislocations. The best graded layers grown by MBE have been grown with mismatch strain rates close to that

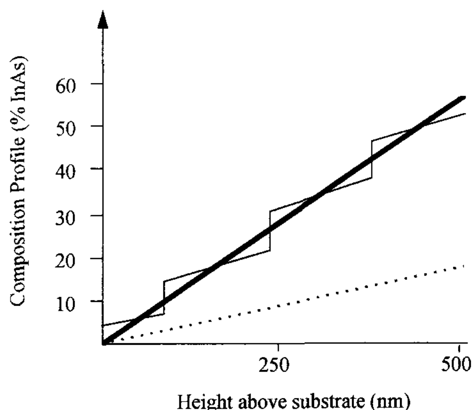


Fig. 9. Schematic diagram illustrating the fastest possible grade rate (bold line) for InGaAs/GaAs. The grower's preferred grade rate for a linear grade is that shown by the dotted line. The single line shows a design to incorporate steps with the preferred grade rate in order to achieve the fastest possible rate.

shown by the dotted line in Fig. 9 (0.03% InAs content/nm).

Additionally we have shown that constant composition layers appear more likely to result in residual strain in lower parts of the structure. For step-graded layers care has to be taken that each layer is thick enough to ensure enough relaxation for the next layer not to present a growth strain in excess of 0.018. Examples of structures where the growth strain has been too great have been presented elsewhere [14,15]. In general, constant composition layers are useful for analysis, e.g. to give discrete peaks in X-ray diffraction, but provide no clear advantage in terms of efficient relaxation. We have shown previously, that in order to reduce the amplitude of surface striations the layers should be as thin as possible.

The single line in Fig. 9 illustrates a structure that we propose to achieve the fastest possible grade rate overall. This consists of graded layers with steps in composition between the layers thus avoiding both the disadvantages of a fast grade and a thick constant composition layer.

## 5. Conclusions

Typical GaAs and InP wafer substrates are expected to have lattice constants with deviations from the mean of $< 100$ ppm. At present it is not possible

to achieve the same tolerances as this with relaxed buffer layers where we achieve lattice parameters with variations up to 1000 ppm. However, it is a useful starting point to be able to give a prediction of the surface lattice parameter and expected crystal quality of a particular design. This work has contributed to an overall strategy in the design of buffer layer structures. In particular, we have shown, subject to stringent growth conditions, that:

- The top surface in-plane lattice parameter of our buffer layers is predictable to within 1000 ppm (0.1%).
- The depth of dislocation-free material at the top of a buffer layer structure is predictable.
- Striation height in InGaAs alloys increases with both the increase in strain relaxation *and* thickness, thus implying that the highest possible grade rate should be used.
- Constant composition layers tend to inhibit dislocation motion at low stresses, implying that low grade rates may lead to residual strains in the structures.
- Composition steps in a graded structure do not present problems providing they do not create a growth strain in excess of 0.018 for subsequent layers.
- Striation heights are a function of relaxation and overgrowth and may be modified by growth conditions.
- Relaxation of all types of grade is accompanied by tilting of the structure, Overgrowth may lead to reduced tilting of the top layer.

## Acknowledgements

This work was funded by the Commission of the European Communities through ESPRIT project No. 6854 (BLES). The Reciprocal Space Maps were obtained courtesy of Dr P.F. Fewster at Philips Research Laboratories, Redhill, UK.

## References

[1] R. Beanland, D.J. Dunstan and P.J. Goodhew, Adv. Phys. 45 (1995) 87.
[2] D.J. Dunstan, P. Kidd, L.K. Howard and R.H. Dixon, Appl. Phys. Lett. 59 (1991) 3390.
[3] D.J. Dunstan, P. Kidd, P.F. Fewster, N.L. Andrew, R. Grey, J.P.R. David, L. González, Y. González, A. Sacedón and F. González-Sanz, Appl. Phys. Lett. 65 (1994) 839.
[4] L.K. Howard, P. Kidd and R.H. Dixon, J. Crystal Growth 125 (1992) 281.
[5] D.J. Dunstan, P. Kidd, R. Beanland, A. Sacedón, E. Calleja, L. González, Y. González and F.J. Pacheco, Mater. Sci. Eng. B, Proc. 1 ICMM, Barcelona, Oct., 1994, submitted.
[6] F.K. LeGoues, MRS Bull. 21 (1996) 38.
[7] A.V. Drigo, A. Aydinli, A. Carnera, F. Genova, C. Rigo, C. Ferrari, P. Franzosi and G. Salviati, J. Appl. Phys. 66 (1989) 1975.
[8] A. Sacedón, F. González-Sanz, E. Calleja, E. Muñoz, S.I. Molina, F.J. Pacheco, D. Araújo, R. Garcia, M. Lourenço, Z. Yang, P. Kidd and D.J. Dunstan, Appl. Phys. Lett. 66 (1995) 3334.
[9] D.J. Dunstan, Philos. Mag. A 73 (1996) 1323.
[10] S.J. Molina, F.J. Pacheco, D. Araújo, R. García, A. Sacedón, E. Calleja, Z. Yang and P. Kidd, Appl. Phys. Lett. 65 (1994) 2460.
[11] D. González, D. Araújo, S.I. Molina, A. Sacedón, E. Calleja and R. Garcia, Mater. Sci. Eng. B 28 (1994) 497.
[12] F. Briones, L. González and A. Ruiz, Appl. Phys. A 49 (1989) 729.
[13] P.F. Fewster, Semicond. Sci. Technol. 8 (1993) 1915.
[14] D.J. Dunstan, R.H. Dixon, P. Kidd, L.K. Howard, V.A. Wilkinson, J.D. Lambkin, C. Jeynes, M.P. Halsall, D. Lancefield, M.T. Emeny, P.J. Goodhew, K.P. Homewood, B.J. Sealy and A.R. Adams, J. Crystal Growth 126 (1993) 589.
[15] V. Krishnamoorthy, P. Ribas and R.M. Park, Appl. Phys. Lett. 58 (1991) 2000.
[16] P. Kidd, D.J. Dunstan, R. Grey, J.P.R. David, P.F. Fewster, N.L. Andrew, S.I. Molina and C.J. Kiely, in: Inst. Phys. Conf. Ser. No. 134: Microsc. Semicond. Mater. Conf., Oxford, April, 1993, Eds. A.G. Cullis, A.E. Staton-Bevan and J.L. Hutchison (IOP, Bristol) pp. 321–324.
[17] J. Tersoff, Appl. Phys. Lett. 62 (1993) 693.
[18] F.K. Le Goues, B.S. Meyerson and J.F. Morar, Phys. Rev. Lett. 66 (1991) 2903.
[19] A.G. Cullis, MRS Bull. 21 (1996) 21.
[20] R. Beanland, M. Aindow, T.B. Joyce, P. Kidd, M. Lourenço and P.J. Goodhew, J. Crystal Growth 149 (1995) 1.
[21] K.L. Kavanagh, M.A. Capano, L.W. Hobbs, J.C. Barbow, P.M.J. Maree, W. Schaff, J.W. Mayer, D. Pettit, J.M. Woodall, J.A. Stroscio and R.M. Feenstra, J. Appl. Phys. 64 (1988) 4843.
[22] P. Kidd and P.F. Fewster, Mater. Res. Soc. Symp. Proc. 317 (1994) 291.
[23] P. Kidd, P.F. Fewster and N.L. Andrew, J. Phys. D: Appl. Phys. 28 (1995) A133.